Article

Journal of
Nanoscience and Nanotechnology
Vol. 17, 1400–1406, 2017
www.aspbs.com/jnn

Nickel-Platinum Nanoparticles Supported on Zeolitic Imidazolate Framework/Graphene Oxide as High-Performance Adsorbents for Ambient-Temperature Hydrogen Storage

Jian Zhang, Dong Ji, Hu Zhou*, Xiufen Yan, and Aihua Yuan*

School of Environmental and Chemical Engineering, School of Material Science and Engineering, Jiangsu University of Science and Technology, Zhenjiang 212003, P. R. China

A facile liquid impregnation method followed by a reduction treatment was applied for loading transition metals nickel, nickel-platinum, and platinum into zeolitic imidazolate framework (ZIF-8)/graphene oxide (GO) as potential adsorbents for ambient-temperature hydrogen storage. These materials have been characterized by powder X-ray diffraction, infrared spectra, scanning electron microscopy, transmission electron microscopy, energy-dispersive X-ray spectroscopy, inductively coupled plasma-emission spectroscopy, and gas adsorption apparatus for their physical and chemical properties. The metal-doped ZIF-8/GO composites maintained the morphology of pristine ZIF-8, although their specific surface areas significantly decreased. The metal nanoparticles in the corresponding composites have average diameters of 4.2–5.1 nm, and uniformly located on the external surface and edges of ZIF-8/GO network. Hydrogen adsorption amounts on metal-doped samples were enhanced by factors of 2.3–3.8 times over ZIF-8 at 298 K due to the spillover effect. Notably, the Pt-doped ZIF-8/GO sample seems to be the best adsorbent for hydrogen storage because of the higher catalytic reactivity of platinum than nickel.

Keywords: Metal-Organic Framework, Graphene Oxide, Nickel, Platinum, Hydrogen Storage, Spillover.

1. INTRODUCTION

Over the past few decades, tremendous efforts have been devoted to the development of metal-organic frameworks (MOFs) in the field of hydrogen storage, due to their merits of ultrahigh porosity, large specific surface areas, together with the adjustable pore sizes and chemical functionalities.[1,2] However, the extraordinary hydrogen adsorption amounts of porous MOFs are achieved only at extremely low temperatures (77 K, 87 K), and decreased noticeably upon elevating temperatures, which can be reasonably ascribed to the weak van der Waals interactions between hydrogen and MOFs. The spillover technique for hydrogen storage has attracted much attention in recent years from the view of practical application.[3–5] Hydrogen spillover is defined as the dissociative chemisorptions of hydrogen molecules on metal catalysts and subsequent migration of atomic hydrogen onto the surface of support.[6,7] Yang group reported that the significantly enhanced hydrogen storage capacities at 298 K have been obtained by physically mixing MOFs and Pt/AC catalysts.[8,9] With this strategy, obvious improvements were evidenced subsequently in other porous MOFs.[10–14]

Graphene oxide (GO) with rich functional groups is very suitable to construct graphene-based hybrids.[15–24] Recently, GO has been successfully combined with MOFs to increase the atomic density of MOFs' surface, and thus to improve the dispersive forces and porosities of the structure. The synergistic effect between both components on the porosity and chemistry of adsorbents led to noticeable enhancements in gas adsorption compared to parent MOFs.[25–29] This inspired our group to employ MOF/GO hybrids as supports to immobilize metal catalysts. As a

*Authors to whom correspondence should be addressed.

 1533-4880/2017/17/1400/007 doi:10.1166/jnn.2017.12685

result, series of Pt-doped MOF/GO composites have been constructed, and significantly evaluated hydrogen storage capacities at 298 K were achieved via spillover.[30–33] As we all know, the cheap nickel nanoparticles (NPs) are also effective as the hydrogen dissociation source. So, the purpose of this work is to investigate the influence of different catalysts (Ni, NiPt, Pt) on hydrogen adsorption performances of the metal-doped MOF/GO system. To the best of our knowledge, Ni- and NiPt-doped MOF/GO composite system has not been reported to date.

2. EXPERIMENTAL DETAILS

2.1. Synthesis

Unless otherwise mentioned, all reactants were used as purchased without further purification. The natural flake graphite purchased from Qingdao Guyu Graphite Co., Ltd., with a particle size of 150 μm (99.9% purity).

2.1.1. Graphene Oxide (GO)

GO was synthesized by oxidation of graphite via a modified Hummers method.[34] Typically, graphite (2.0 g) was added to concentrated H_2SO_4 (80 mL) and stirred in an ice bath. Then, $NaNO_3$ (4.0 g) and $KMnO_4$ (8.0 g) were gradually added under stirring at below 10 °C. The reaction mixture was continually stirred for 4 h at below 10 °C. Successively, the mixture was stirred at 35 °C for another 4 h, and then diluted with deionized (DI) water (200 mL). The addition of DI water was carried out in an ice bath to keep temperatures below 100 °C. The mixture was further stirred for 1 h after adding all DI water. The reaction was then terminated by adding 30% H_2O_2 solution (15 mL). The mixture was left overnight, and the solid product was separated by centrifugation, washed repeatedly with 5% HCl solution until sulfate could not be detected with $BaCl_2$. For further purification, the resulting solid was redispersed in DI water and then was dialyzed for 72 h to remove residual salts and acids. The suspension was dried in a vacuum oven at 60 °C for 24 h to obtain GO.

2.1.2. ZIF-8

ZIF-8 was prepared by using a reported procedure.[35] In a typical synthesis procedure, a methanol solution (25 mL) of $Zn(NO_3)_2 \cdot 6H_2O$ (1.25 mmol) was slowly added into a methanol solution (25 mL) of 2-methylimidazole (10.00 mmol) with constant stirring. Stirring was stopped after combining the component solutions and a gel-like solid was recovered by centrifugation and washed with methanol for three times. Finally, the products were dried at 60 °C overnight.

2.1.3. ZIF-8/GO

ZIF/GO was obtained by dispersing a certain amount of GO (5 wt% of the final material) in the well-dissolved ZIF-8 precursors and solvent mixture. The resultant suspension was subsequently centrifuged, washed several times with water-methanol mixture solvent and then dried at 60 °C.

2.1.4. NiPt@ZIF-8/GO

To incorporate metallic Ni and/or Pt into ZIF-8/GO, a simple liquid impregnation method was used according to our developed procedure.[30] Prior to metal loading, the ZIF-8/GO sample was activated under vacuum at 160 °C for 24 h to remove solvent or guest molecules involved in the framework. The activated ZIF-8/GO sample was impregnated with the aqueous solution containing catalyst precursors. A total of Ni and Pt metals in the final products is theoretically 5 wt% at different Ni/Pt mass ratios (5/0, 2.5/2.5, 0/5). Here a typical synthetic procedure for Ni@ZIF-8/GO is described in detail. An aqueous solution (20 mL) of $Ni(NO_3)_2 \cdot 6H_2O$ (49.53 mg) was first mixed with polyvinyl alcohol (PVA) (22.58 mg) and continuously stirred for 1 h at 25 °C. 200 mg of freshly activated ZIF-8/GO sample was added to above solution, and the mixture was stirred for 2 hours to impregnate metal salts. After the impregnation, an aqueous solution (4.8 mL) of $NaBH_4$ (30 mg) was added dropwise to the reaction suspension in an ice bath with vigorous stirring. After further stirring for 5 hours, the precipitations were isolated by filtration, and washed thoroughly with deionized water/methanol. Finally, the resulting products were dried overnight at 60 °C. The Ni content on the sample was 4.52 wt% based on ICP analysis. The Pt@ZIF-8/GO sample was obtained by following the analogous process except for using $H_2PtCl_6 \cdot 6H_2O$, where the actual Pt content was 4.34 wt%. To synthesize NiPt@ZIF-8/GO, the salts $Ni(NO_3)_2 \cdot 6H_2O$ and $H_2PtCl_6 \cdot 6H_2O$ were both used, and the actual Ni and Pt contents on the sample were 2.37 and 2.44 wt%, respectively.

2.2. Characterization

Powder X-ray diffraction (XRD) patterns of all samples were collected on a Shimadzu XRD-6000 diffractometer

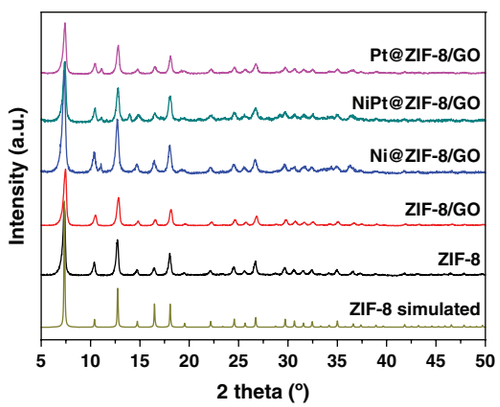

Figure 1. Powder XRD patterns of ZIF-8, ZIF-8/GO, and NPs@ZIF-8/GO samples.

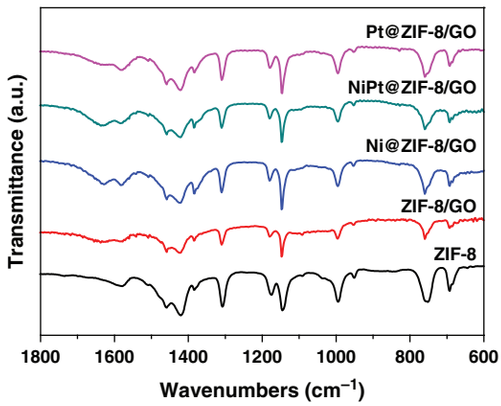

Figure 2. IR spectra of ZIF-8, ZIF-8/GO, and NPs@ZIF-8/GO samples.

with Cu-K_α radiation source ($\lambda = 0.154178$ nm). Infrared (IR) spectra were measured on a Nicolet FT 1703X spectrometer in the 4000–400 cm^{-1} region (KBr pellets). The metallic contents of Ni and Pt were determined by an Agilent 7700 inductively coupled plasma-emission spectroscopy (ICP-MS). The morphologies and sizes were observed by using a field-emission scanning electron microscope (FE-SEM, ZEISS Merlin Compact) and high-resolution transmission electron microscopy (HR-TEM, JEOL JEM-2100F). The elemental mapping distributions were examined by energy-dispersive X-ray spectrometry (EDS, Oxford X-Max). The nitrogen and hydrogen adsorption isotherms were recorded on automatic volumetric adsorption equipment (Micromeritics ASAP 2020). Prior to experiments, the as-prepared samples were evacuated at 160 °C for 12 h. UHP grade N_2 and H_2 (99.999%) gases were used for all measurements. The Brunauer–Emmett–Teller (BET) specific surface areas were calculated using adsorption data in the relative pressure P/P_0 of 0.06–0.30. The total pore volume was estimated by a single point method at P/P_0 of 0.99.

3. RESULTS AND DISCUSSION

3.1. Structural Characterization

The characteristic XRD peaks of as-prepared ZIF-8 match well with those derived from single-crystal XRD data,[36] confirming the successful preparation of the same MOF. The diffraction patterns of all composites revealed no loss of crystallinity, as shown in Figure 1, which indicates that the structural integrity of ZIF-8 framework was been maintained well after the incorporation of GO and metal NPs. The diffraction patterns of metal-doped ZIF-8/GO composites did not exhibit characteristic peaks for metal species, probably as a result of the formation of very small sizes of NPs. This assumption is consistent with TEM observations described below.

All composites exhibit identical infrared spectra bands (Fig. 2) to pristine ZIF-8, suggesting that the immobilizing of GO and metal NPs did not prevent the formation of MOF framework, as determined by XRD analysis. The adsorption bands at around 1581 cm^{-1} are reasonably assigned to the C═N stretching vibrations of the imidazole ligands, while the intense and convoluted bands at 1500–1350 cm^{-1} are associated with the entire ring stretching. Furthermore, the in-plane and out-of-plane bending of the ring can be observed in the region of 1350–900 cm^{-1} as well as below 800 cm^{-1}. The fingerprint bands of GO component were not observed in composites because of the much lower contents.

3.2. Morphological Characterization

The morphologies and sizes of all samples were characterized by SEM images, as shown in Figure 3. GO has a typical crumpled layered structure, whereas ZIF-8

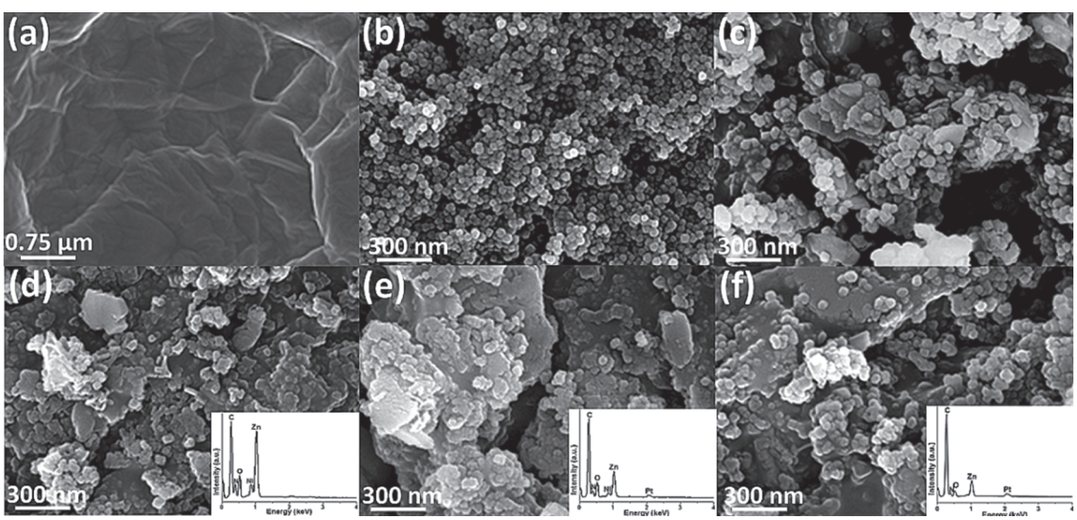

Figure 3. SEM images of (a) GO, (b) ZIF-8, (c) ZIF-8/GO, (d) Ni@ZIF-8/GO, (e) NiPt@ZIF-8/GO, and (f) Pt@ZIF-8/GO.

nanocrystals in ZIF-8/GO and NPs@ZIF-8/GO samples are randomly dispersed on GO sheets. The EDS analysis confirmed the presence of Ni and/or Pt species despite the fact that these NPs cannot be observed from SEM images because of their very small sizes. The corresponding elemental mapping distribution indicated the high dispersion of Ni and/or Pt NPs into the ZIF-8/GO network (Fig. 4) and the absence of any aggregation. ICP analysis indicated that the measured contents of Ni and Pt are close to the theoretical ones (Table I).

One can see from TEM images (Fig. 5) that ZIF-8 crystals have well-defined hexagonal structures with the uniform shape and size in the range of 40–50 nm. No significant changes in the morphology occurred upon the construction of ZIF-8/GO and metal-doped ZIF-8/GO. The metal NPs in metal-doped ZIF-8/GO composites were uniformly dispersed into the ZIF-8/GO network and no obvious aggregation of NPs were observed. In fact, the presence of GO may be a contributing factor because GO sheets can provide platforms for the well dispersion of metal species despite a quite small content in the whole composite. The high magnification TEM images (Fig. 6) of metal NPs reveals that these particles exist as black dots with average sizes of approximately 4.3(Ni), 5.1(NiPt), and 4.2(Pt) nm calculated from a statistical evaluation of 80–100 particles. The diameters of NPs are much larger than pore sizes (1.16 nm, 0.34 nm) of ZIF-8.[26] So the loaded metal species are not encapsulated in the cages of ZIF-8 but located on the external surface and edges of ZIF-8 and GO.

Table I. Specific surface areas, pore volumes, and hydrogen uptakes at 298 K for ZIF-8, ZIF-8/GO, and NPs@ZIF-8/GO samples.

Samples	NPs loadings (wt%)	S^a_{BET} ($m^2\ g^{-1}$)	V^b_{total} ($cm^3\ g^{-1}$)	H_2 uptake (298 K, 860 mmHg) (mmol g^{-1})
ZIF-8	0	1297	1.225	0.036
ZIF-8/GO	0	1247	1.281	0.034
Ni@ZIF-8/GO	4.52 (Ni)	923	0.691	0.084
NiPt@ZIF-8/GO	2.37 (Ni), 2.44 (Pt)	858	0.616	0.129
Pt@ZIF-8/GO	4.34 (Pt)	1008	0.843	0.135

Notes: [a]S_{BET} is the BET specific surface area; [b]V_{total} is the total pore volume calculated from single point adsorption data.

3.3. Textural Characterization

The specific surface areas were determined by nitrogen physisorption measurements (Fig. 7, Table I). In comparison with 1297 $m^2\ g^{-1}$ of pure ZIF-8, the BET specific surface area for ZIF-8/GO was 1247 $m^2\ g^{-1}$. The BET value of as-synthesized ZIF-8 is close to those observed in literatures [37–39]. Notably, the value measured for ZIF-8/GO is slightly higher than the hypothetical one (1232 $m^2\ g^{-1}$) calculated by physically mixing GO and

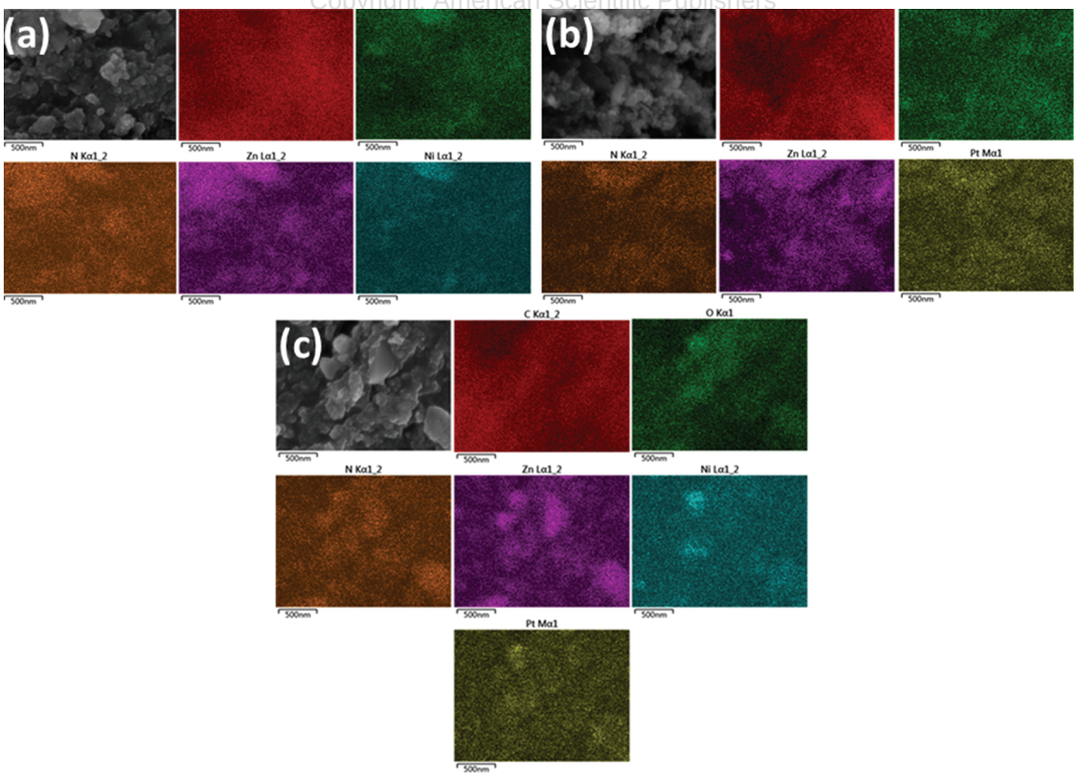

Figure 4. Elemental mapping distribution for (a) Ni@ZIF-8/GO, (b) Pt@ZIF-8/GO, and (c) NiPt@ZIF-8/GO.

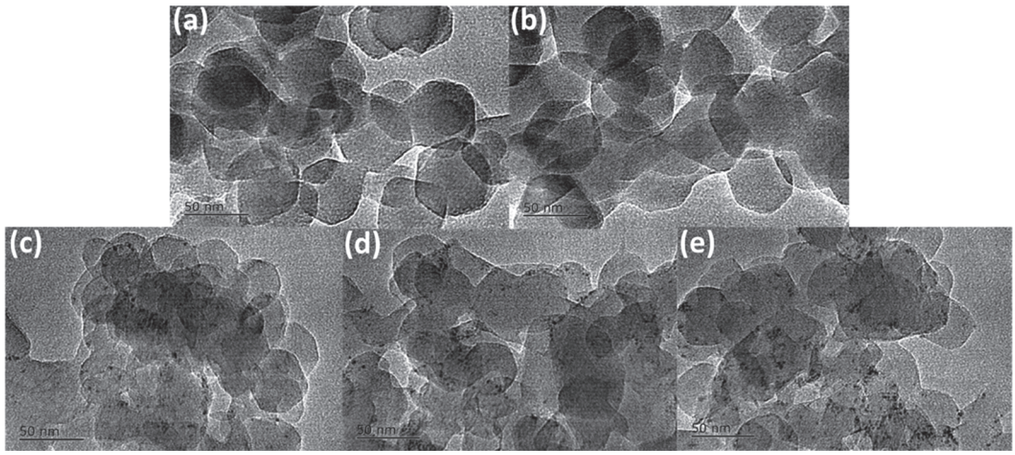

Figure 5. TEM images of (a) ZIF-8, (b) ZIF-8/GO, (c) Ni@ZIF-8/GO, (d) NiPt@ZIF-8/GO, and (e) Pt@ZIF-8/GO.

ZIF-8. This can be attributed to the synergistic effect between GO and MOF components, as observed in other MOF/GO materials.[25, 29, 40] It should be mentioned here that the appreciable decrease of BET values and pore volumes between metal-doped ZIF-8/GO and ZIF-8 strongly demonstrated that the cavities of host ZIF-8 were blocked by highly dispersed metal NPs since the diameters of metal NPs are much larger than pore sizes of ZIF-8, as in the case of NPs-loaded MOFs.[41, 42]

3.4. Hydrogen Adsorption Performance

Hydrogen adsorption isotherms at 298 K for ZIF-8, ZIF-8/GO, and metal-doped ZIF-8/GO samples are presented in Figure 8. ZIF-8 and ZIF-8/GO have hydrogen storage capacities of 0.036 and 0.034 mmol g^{-1} (298 K, 860 mmHg), respectively. The measured value for as-prepared ZIF-8 is close to the reported one under the similar condition.[43] By doping metal NPs, hydrogen uptakes under the same condition for Ni-, NiPt-, and Pt-doped samples are 0.084, 0.129, and 0.135 mmol g^{-1}, respectively. It was observed that adsorption amounts of all composites are much higher than that of ZIF-8 or ZIF-8/GO, and the enhancement factors for these composites over pristine ZIF-8 are in the range of 2.3–3.8 times. As shown in nitrogen adsorption curves, the BET values and pore volumes of metal-doped composites noticeably decreased upon the incorporation of metal catalysts relative to ZIF-8 and ZIF-8/GO, which indicated that the improvement of hydrogen storage capacities should be mainly attributed to the spillover effect caused by metal catalysts. The metal NPs (Ni, Pd, Pt, Ru, Co, etc.) are effective as the hydrogen dissociation source, and the increased hydrogen adsorption performance has been documented in metal-doped carbon-based adsorbents.[44–47] Here it is necessary to investigate the contribution of metal NPs and ZIF-8/GO support on this unusually increase in hydrogen uptakes, in order to clearly understand the hydrogen spillover mechanism involve in our system. In general, such an improvement can be mainly ascribed to the high catalytic efficiency of metal catalysts on dihydrogen at ambient temperature. In our case, the spillover effect may promote the dissociation of molecular hydrogen

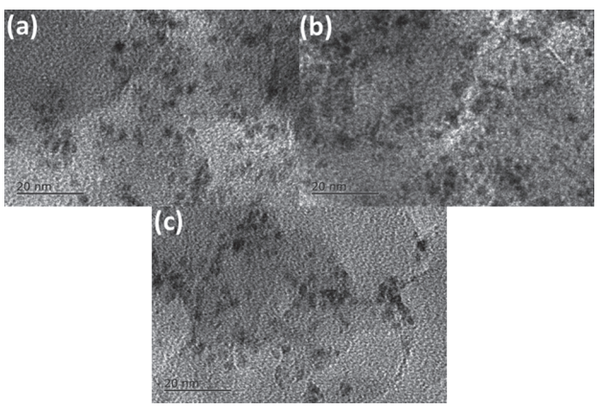

Figure 6. TEM images of (a) Ni NPs in Ni@ZIF-8/GO, (b) NiPt NPs in NiPt@ZIF-8/GO, and (c) Pt NPs in Pt@ZIF-8/GO.

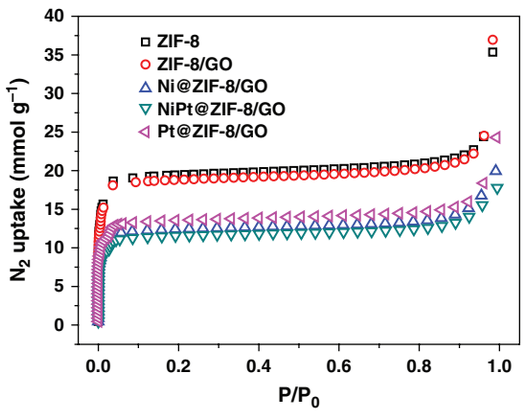

Figure 7. Nitrogen adsorption isotherms at 77 K of ZIF-8, ZIF-8/GO, and NPs@ZIF-8/GO samples.

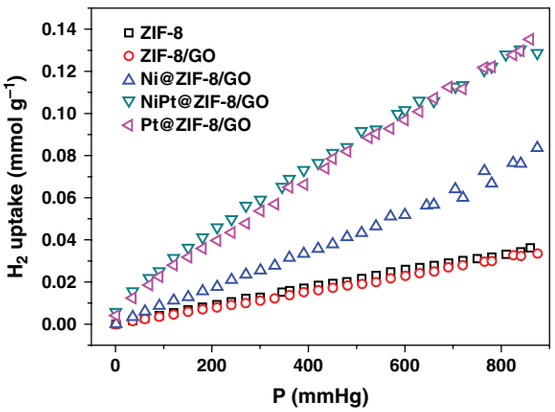

Figure 8. Hydrogen adsorption isotherms at 298 K of ZIF-8, ZIF-8/GO, and NPs@ZIF-8/GO samples.

on the surface of Ni and/or Pt NPs, and then a further diffusion of monatomic hydrogen to cavities and surfaces of the ZIF-8/GO network, where hydrogen atoms are chemically bounded. The hydrogen uptakes in composites follow the order of Pt@ZIF-8/GO > NiPt@ZIF-8/GO > Ni@ZIF-8/GO. The best performance observed in Pt@ZIF-8/GO may be attributed to the higher catalytic reactivity of Pt than Ni, where Pt catalysts are better for the adsorption and dissociation of molecular hydrogen on the catalyst surface. Thus, the loading of NiPt is also more beneficial to the diffusion of dissociated atomic hydrogen than pure Ni doping. In addition, the oxygen functional groups on GO sheets, the large surface area of ZIF-8 as well as the synergistic effect between ZIF-8 and GO components also facilitate the anchoring and dispersion of metal catalysts on the ZIF-8/GO network. The role of oxygen groups from the receptor in improving hydrogen adsorption capacities via spillover has been documented in other materials.[48–50] Thus, the contribution for hydrogen adsorption via spillover onto the GO surface could not be ignored despite the much low weight ratio (5 wt%) of GO to ZIF-8.

4. CONCLUSIONS

In summary, metal NPs (Ni, NiPt, Pt)-doped ZIF-8/GO composites were prepared by a simple liquid impregnation approach followed by a reduction treatment. The metal catalysts uniformly located on the external surface and edges of ZIF-8/GO network. Notably, the loading of metal NPs led to a significant enhancement in the ambient-temperature hydrogen storage capacities relative to pure ZIF-8, and this unusual improvement can be reasonably attributed to the spillover mechanism. It was found that the higher catalytic reactivity of Pt than Ni resulted in the best hydrogen adsorption performance observed in the Pt-doped samples. The present work demonstrates the feasibility of metal-doped MOF/GO as a potentially practical candidate for hydrogen storage. To look for cheap catalysts together with the optimization of loading strategies are our main research directions based on hydrogen spillover enhancement effect in future.

Acknowledgments: This work was financially supported by the National Natural Science Foundation of China (51102119, 51272095), Natural Science Foundation of Jiangsu Province (BK20151328), Qing Lan Project of Jiangsu Province, the project of the Priority Academic Program Development of Jiangsu Higher Education Institutions, China Postdoctoral Science Foundation (2014M561578) and Jiangsu Planned Projects for Postdoctoral Research Funds (1401109C).

References and Notes

1. H. Furukawa, K. E. Cordova, M. O'Keeffe, and O. M. Yaghi, *Science* 341, 1230444 (**2013**).
2. M. P. Suh, H. J. Park, T. K. Prasad, and D. W. Lim, *Chem. Rev.* 12, 782 (**2012**).
3. L. F. Wang, A. J. Lachawiec, Jr., and R. T. Yang, *RSC Adv.* 3, 13935 (**2013**).
4. L. F. Wang and R. T. Yang, *Catal. Rev.* 52, 411 (**2010**).
5. L. F. Wang and R. T. Yang, *Energ. Environ. Sci.* 1, 268 (**2008**).
6. S. T. Srinivas and P. K. Rao, *J. Catal.* 148, 470 (**1994**).
7. A. J. Robell, E. V. Ballou, and M. Boudart, *J. Phys. Chem.* 68, 2748 (**1964**).
8. Y. W. Li and R. T. Yang, *J. Am. Chem. Soc.* 128, 8136 (**2006**).
9. Y. W. Li and R. T. Yang, *J. Am. Chem. Soc.* 128, 726 (**2006**).
10. S. N. Klyamkin, S. V. Chuvikov, N. V. Maletskaya, E. V. Kogan, V. P. Fedin, K. A. Kovalenko, and D. N. Dybtsev, *Int. J. Energ. Res.* 38, 1562 (**2014**).
11. S. Y. Lee and S. J. Park, *Int. J. Hydrogen Energy* 36, 8381 (**2011**).
12. Y. W. Li and R. T. Yang, *Langmuir* 23, 12937 (**2007**).
13. Y. W. Li and R. T. Yang, *AIChE J.* 54, 269 (**2008**).
14. Y. Y. Liu, J. L. Zeng, J. Zhang, F. Xu, and L. X. Sun, *Int. J. Hydrogen Energy* 32, 4005 (**2007**).
15. B. H. Kim, S. H. Lee, S. W. Han, S. Ahn, J. Noh, and J. B. Park, *Mater. Express* 6, 61 (**2016**).
16. F. H. Li, X. Y. Xu, Z. W. Shen, M. Q. Yang, and W. Wang, *Sci. Adv. Mater.* 7, 2410 (**2015**).
17. A. Mondal and N. Jana, *Rev. Nanosci. Nanotechnol.* 3, 177 (**2014**).
18. Z. P. Li, G. Q. Tan, Y. L. Cui, J. Li, Q. Zhao, M. Li, Y. F. Chang, H. Y. Yuan, and D. Xiao, *Nanosci. Nanotechnol. Lett.* 6, 1063 (**2014**).
19. M. S. Fu and J. G. Li, *Nanosci. Nanotechnol. Lett.* 6, 1116 (**2014**).
20. M. C. Liu, X. L. Wu, C. L. Chen, Q. Wang, T. Wen, and X. K. Wang, *Sci. Adv. Mater.* 5, 1686 (**2013**).
21. Q. Mi, J. C. Hu, M. Luo, Z. X. Huang, and J. L. Li, *Sci. Adv. Mater.* 5, 1649 (**2013**).
22. L. H. Tian, C. Q. Gong, J. Y. Liu, L. Q. Ye, and L. Zan, *Sci. Adv. Mater.* 5, 1627 (**2013**).
23. J. Ni, X. K. Yuan, and H. H. Liu, *Nanosci. Nanotechnol. Lett.* 5, 654 (**2013**).
24. S. T. Yang, J. B. Luo, J. H. Liu, Q. H. Zhou, J. Wan, C. Ma, R. Liao, H. F. Wang, and Y. F. Liu, *Nanosci. Nanotechnol. Lett.* 5, 372 (**2013**).
25. R. Kumar, K. Jayaramulu, T. K. Maji, and C. N. R. Rao, *Chem. Commun.* 49, 4947 (**2013**).
26. I. Ahmed, N. A. Khan, and S. H. Jhung, *Inorg. Chem.* 52, 14155 (**2013**).
27. C. Petit and T. J. Bandosz, *Adv. Funct. Mater.* 21, 2108 (**2011**).
28. M. Jahan, Q. L. Bao, J. X. Yang, and K. P. Loh, *J. Am. Chem. Soc.* 132, 14487 (**2010**).
29. C. Petit and T. J. Bandosz, *Adv. Mater.* 21, 4753 (**2009**).

30. H. Zhou, J. Zhang, J. Zhang, X. F. Yan, X. P. Shen, and A. H. Yuan, *Int. J. Hydrogen Energy* 40, 12275 **(2015)**.
31. H. Zhou, J. Zhang, J. Zhang, X. F. Yan, X. P. Shen, and A. H. Yuan, *Inorg. Chem. Commun.* 54, 54 **(2015)**.
32. H. Zhou, X. Q. Liu, J. Zhang, X. F. Yan, Y. J. Liu, and A. H. Yuan, *Int. J. Hydrogen Energy* 39, 2160 **(2014)**.
33. J. Zhang, X. Q. Liu, H. Zhou, X. F. Yan, Y. J. Liu, and A. H. Yuan, *RSC Adv.* 4, 28908 **(2014)**.
34. W. S. Hummers and R. E. Offeman, *J. Am. Chem. Soc.* 80, 1339 **(1958)**.
35. J. Cravillon, S. Münzer, S. J. Lohmeier, A. Feldhoff, K. Huber, and M. Wiebcke, *Chem. Mater.* 21, 1410 **(2009)**.
36. K. S. Park, Z. Ni, A. P. Côté, J. Y. Choi, R. Huang, F. J. Uribe-Romo, H. K. Chae, M. O'Keeffe, and O. M. Yaghi, *P. Natl. Acad. Sci. USA* 103, 10186 **(2006)**.
37. T. T. Dang, Y. H. Zhu, J. S. Y. Ngiam, S. C. Ghosh, A. Chen, and A. M. Seayad, *ACS Catal.* 3, 1406 **(2013)**.
38. L. H. Wee, N. Janssens, S. P. Sree, C. Wiktor, E. Gobechiya, R. A. Fischer, C. E. A. Kirschhock, and J. A. Martens, *Nanoscale* 6, 2056 **(2014)**.
39. P. Wang, J. Zhao, X. B. Li, Y. Yang, Q. H. Yang, and C. Li, *Chem. Commun.* 49, 3330 **(2013)**.
40. C. Petit, J. Burress, and T. J. Bandosz, *Carbon* 49, 563 **(2011)**.
41. C. Rosler and R. A. Fischer, *CrystEngComm.* 17, 199 **(2015)**.
42. H. R. Moon, D. W. Lim, and M. P. Suh, *Chem. Soc. Rev.* 42, 1807 **(2013)**.
43. W. Zhou, H. Wu, M. R. Hartman, and T. Yildirim, *J. Phys. Chem. C* 111, 16131 **(2007)**.
44. D. Saha and S. G. Deng, *Langmuir* 25, 12550 **(2009)**.
45. L. F. D'Elia, G. I. Saavedra, and V. Gottberg, *Int. J. Hydrogen Energy* 34, 1958 **(2009)**
46. L. F. Wang and R. T. Yang, *J. Phys. Chem. C* 112, 12486 **(2008)**.
47. E. A. Ivanova Shor, V. A. Nasluzov, A. M. Shor, G. N. Vayssilov, and N. Rösch, *J. Phys. Chem. C* 111, 12340 **(2007)**.
48. T. Y. Chung, C. S. Tsao, H. P. Tseng, C. H. Chen, and M. S. Yu, *J. Coll. Interf. Sci.* 441, 98 **(2015)**.
49. Q. Li and A. D. Lueking, *J. Phys. Chem. C* 115, 4273 **(2011)**.
50. Z. Wang, F. H. Yang, and R. T. Yang, *J. Phys. Chem. C* 114, 1601 **(2010)**.

Received: 26 November 2015. Accepted: 21 December 2015.